

Self-Heating Induced Instability of a Non-Linear Inductor in a SMPS: a Case Study.

Daniele Scirè¹, Giuseppe Lullo¹, Gianpaolo Vitale²

¹ Department of Engineering, University of Palermo, 90128 Palermo, Italy {daniele.scire, giuseppe.lullo (at) unipa.it}

² ICAR, Institute for high performance computing and networking, National Research Council (CNR),
 Via Ugo La Malfa, 153, 90146 Palermo {gianpaolo.vitale (at) icar.cnr.it}

Abstract. This paper proposes a case study to show that the non-linear operation of a power inductor in a SMPS can induce instability of the control system leading to overheating of the inductor beyond its allowable temperature and to an excessive peak of the maximum current.

The case study is performed by a commercial ferrite inductor employed in a synchronous boost converter encompassing a control system to adjust the duty cycle, assuring a constant output voltage. The thermal transient is described by the time domain waveforms and thermal images.

Key words. Non-linear inductor, ferrite inductor, magnetic saturation, stability, power density, switched mode power supply.

1. Introduction

Among the solutions aimed at increasing the power density of the Switched Mode Power Supplies (SMPSs), the use of power inductors beyond the linear zone has been receiving increasing interest. It is due to the possibility of saving the size, weight, and cost of the inductor [1, 2]. On the other hand, some issues have to be considered: they are tied to the need of suitable models to describe the inductor's behaviour, thermal management and EMI filter design. Several papers have been dedicated to the model of power inductors describing saturation: the survey [3] addresses analytical models where the inductor is described by a relationship giving the inductance versus current. A model based on trigonometric functions is proposed by [4] and one based on a polynomial function is described in [5]; a comparison between the two models is proposed by [6]. Papers [7, 8] put in evidence the need for a dedicated measurement system since many information to characterize the inductor is not always provided by manufacturers. Thermal phenomena are discussed in [9, 10] and EMI issues are explained in [11, 12]. All the above-cited papers explain the advantages of using non-linear inductors and address design criteria considering the main issues.

A problem not yet addressed in the literature concerns the thermal instability induced by the behaviour of the inductor.

The novelty of this paper consists on the analysis of the intrinsic unstable condition and giving an analytical expression of coefficients belonging to stability threshold.

A practical example is discussed in this paper by a case study in which the non-linear inductor is adopted in a boost converter. The evolution of the temperature is compared considering the linear and non-linear operation of the inductor, respectively. An experimental test shows that the temperature can exceed the maximum value in non-linear operation, leading to a degradation of the component. Results are given both by time domain waveform, to show the increase of the maximum current, and by thermal images to describe the temperature distribution in the SMPS.

2. Internal feedback in non-linear inductors

As it is known, the operation of a linear inductor in an SMPS is based on two different voltages applied to the same inductor during the turn-on and the turn-off time of the power switch. Consequently, the inductor is charged and discharged; it experiences a DC current with superimposed triangular AC waveform. The inductance remains constant during operation, the maximum current depends both on the inductance and the duration of T_{ON} according to:

$$\Delta i_L = i_{L,max} - i_{L,min} = \frac{1}{L} \int_0^{T_{ON}} V_L dt = \frac{V_L T_{ON}}{L} \quad (1)$$

$$i_{L,max} = \bar{i}_L + \frac{\Delta i_L}{2} \quad (2)$$

Where V_L is the voltage at the inductor terminals and the mean current \bar{i}_L depends on the load. The power dissipated into the inductor, considering the Joule effect, is given by eq. (3) where in the root mean square of the AC component, the contribution of the inductance L and T_{ON} is recognizable:

$$P_J = \left[\bar{i}_L^{-2} + \left(\frac{V_L T_{ON}}{L \sqrt{12}} \right)^2 \right] r_L \quad (3)$$

In non-linear operation, when current increases the inductance is lowered, thus further increasing the current and the temperature. The increase in temperature is generally more relevant than the linear operation due to the augmented losses. As a consequence, the inductance value in eq. (1) decreases, hence the maximum current rises, increasing losses and reducing the output voltage. The increase of the duty cycle imposed by the feedback control to compensate for the output voltage drop corresponds to an increase of T_{ON} and, therefore, to a further increase of the maximum current. The instability is demonstrated considering that in non-linear operation an increase in the inductor's temperature implies a further increase of the current peak. As a consequence, the inductor's temperature can tend to a constant value exceeding the rated one or diverge.

The internal feedback is schematized in Fig. 1. The rated inductor value L_0 represents the starting inductance when the core is in equilibrium with the environment (room temperature). The coefficient k_1 represents eq. (3); it gives the Joule losses dissipated within the inductor. In order to simplify the analysis, eq. (3) can be approximated considering losses depending on the square of DC current only.

$$P_J \approx \bar{i}_L^{-2} r_L = k_1 \quad (4)$$

This coefficient is intrinsically positive. Due to the thermal constant of the inductor τ , the temperature increases as in a first-order system. The increase of the core temperature gives the variation of the inductance through the coefficient k_2 . It can be derived from the model of the inductor. Adopting the polynomial model as in [8],

$$L(i_L, T_{core}) = \begin{cases} \sum_{m=0}^3 L_m (1 + \beta_m T_{core}) i_L^m & , L(i_L) > L_{deepsat} \\ L_{deepsat} & , otherwise \end{cases} \quad (5)$$

it follows that:

$$\frac{\partial L}{\partial T} = L_0 \beta_0 + L_1 \beta_1 \bar{i}_L + L_2 \beta_2 \bar{i}_L^{-2} + L_3 \beta_3 \bar{i}_L^{-3} = k_2 \quad (6)$$

The coefficient k_2 depends on the current as well. Its parameters β are negative since increasing the temperature the inductance is lowered. At the end of the loop, the inductance will be $L_0 - \Delta L$ where ΔL is defined by the incremental model of the inductor.

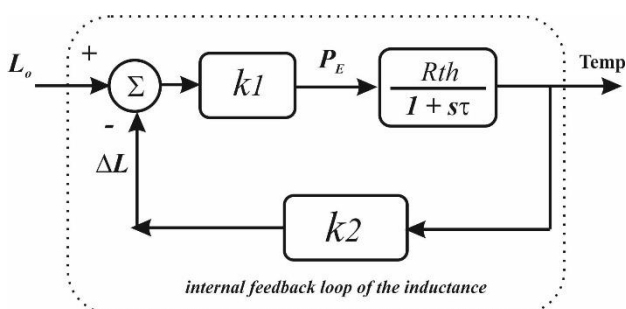


Fig. 1. Block diagram representing the internal loop of the inductor

It can be noted that for a linear inductor, no internal loop exists since no inductance variation occurs; differently, in non-linear case, the greater the temperature, the larger the inductance decrease.

By performing few calculations it is possible to obtain the closed-loop transfer function of the inductor's temperature:

$$G = \frac{k_1 R_{th}}{\tau} \frac{1}{\left(\frac{1 + k_1 k_2 R_{th}}{\tau} \right) + s} \quad (7)$$

From (7) the thermal stability condition is retrieved:

$$k_1 \cdot k_2 > -\frac{1}{R_{th}} \quad (8)$$

It should be noted that increasing the load current, k_1 and k_2 can lead to a system no longer satisfying (8) and thus to instability. Besides, the role of the thermal resistance is crucial: a low thermal resistance extends the stable safe operating area. Obviously, the PCB layout can influence this value. The stable and unstable operations will be shown in this paper by a practical case study.

3. The test rig

The test has been performed on the LM5122EVM-1PH Evaluation Module (EVM) shown in Fig. 2 [13]. The board implements a synchronous boost converter; it employs the Texas Instruments LM5122 synchronous boost controller IC. The circuit is controlled to give 24 V as output with a maximum current of 4.5 A with an input voltage ranging from 9 V to 20 V. The power MOSFETs are N-CH 40 V 100 A by NXP semiconductor PSMN4R0-40YS. The operation mode is set to "forced PWM"; other operations can be set to improve efficiency at light load. The switching frequency is set to 260 kHz as the default value. The Coilcraft DO5010H-104 inductor has been chosen; it is an SMT Power inductor wound on a ferrite core with a rated value of 100 μ H [14]. The manufacturer specifies for the inductor DO5010H 104 a 10% linear threshold current (intended by the same manufacturer as the DC current at which the inductance drops 10% from its rated value) of 3 A. It means that the inductance can be considered constant up to about this value. However, we will extend this range by adopting a 50% saturation current i.e., the current where the differential inductance is reduced to half of its maximum value. It corresponds to a maximum current of about 4 A.

The inductor has been characterized by retrieving the curve of inductance versus current by a dedicated measurement system [8], as represented by the characteristic curves of Fig. 3. The coefficients corresponding to eq. (5) are given in Table I.

Table I - Parameters of the inductor DO5010H-104

L_0	$103.4 \cdot 10^{-6}$	β_0	-0.001332
L_1	$-28.38 \cdot 10^{-6}$	β_1	-0.01273
L_2	$19.86 \cdot 10^{-6}$	β_2	-0.01027
L_3	$-3.563 \cdot 10^{-6}$	β_3	-0.003064

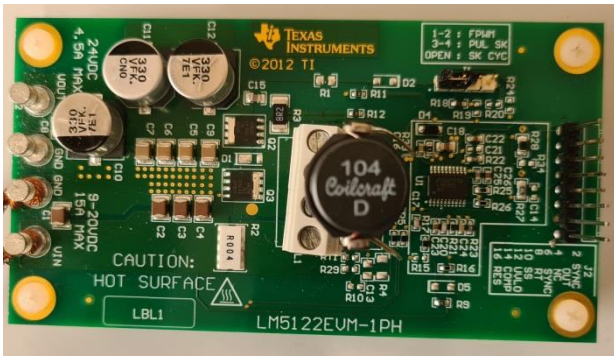


Fig. 2. View of the LM5122EVM-1PH Evaluation Module (EVM) used for the test equipped with the DO5010H-104 ferrite inductor.

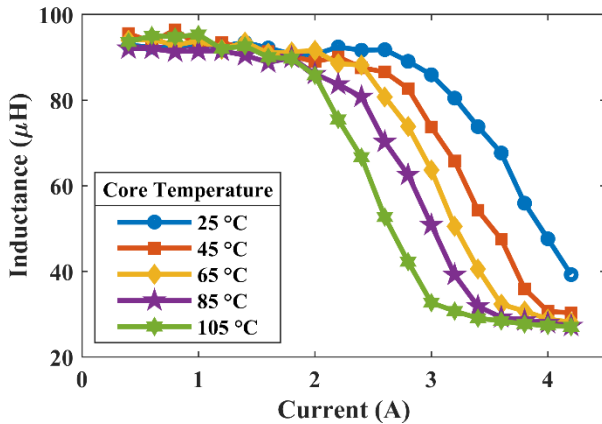


Fig. 3. The characteristic curve of the inductance versus current for the inductor DO5010H-104 experimentally obtained parametrized with temperature [8].

The test rig encompasses a DC linear power supply (12 V, 10 A), a digital oscilloscope TEKTRONIK MSO2024B, equipped with a current probe TEKTRONIK TCP0020. Finally, a thermal imaging camera FLIR C5 is used in this study to measure the temperature of the inductor.

4. Results

Two tests are proposed aiming to show the stable and unstable behaviour based on eq. (8). The former is focused on the linear operation imposing a current in the range suggested by the manufacturer for which eq. (8) is satisfied. The latter shows what happens when the inductor current is increased and the operation is in non-linear zone. In this case, the temperature transient highlights that the inductor's temperature increases lowering the inductance, and causing instability. The corresponding current waveforms are shown to recognize the non-linear operation. The temperatures are acquired by thermal images whose measuring point is placed on the inductor; a discussion on thermal analysis is given in the following section. Figure 4 shows a photograph of the board with the inductor taken with the digital sensor (visible spectrum) of the FLIR camera.



Fig. 4. Photograph, taken with the digital sensor (visible spectrum) of the FLIR camera, of the converter equipped with the inductor under test.

A. Linear operation

The linear operation of the inductor is obtained by imposing a mean current in the inductor of about 1 A. It corresponds to a load resistance of 50 Ω supplied by 24 V with a duty cycle of 50 %.

The test starts at environmental temperature; Figure 5 shows the screenshot of the oscilloscope in which the well-known triangular waveform of the current can be recognized. The inductance value imposes the ripple.

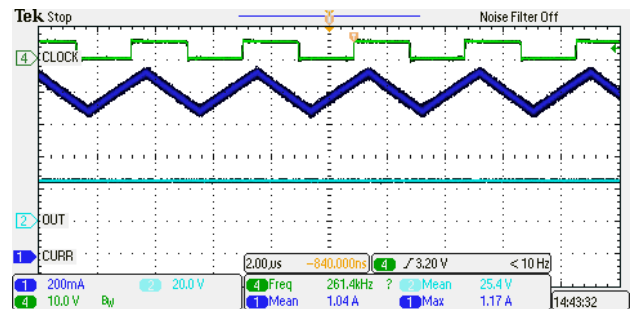


Fig. 5. Output voltage and inductor current through the inductor at environmental temperature

After a transient of 900s the temperature of the inductor reaches 38.3 °C; no relevant variation of the inductance occurs. Consequently, the current waveform remains the same showing the same mean and maximum value as shown in Fig. 6.

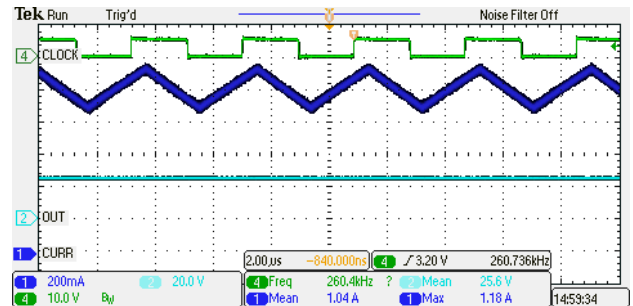


Fig. 6. Output voltage and inductor current through the inductor at the end of the test in linear operation when the inductor's temperature reached 38.3 °C.

B. Non-linear operation

The non-linear operation of the inductor is obtained by increasing its mean current up to about 3.3 A. It corresponds to a load resistance of 16 Ω supplied by 24 V

with a duty cycle of the converter of 50%. The test starts at environmental temperature; Fig. 7 shows a screenshot of the oscilloscope in which the well-expected triangular waveform of the current is recognized; the ripple is about 0.38 A peak-to-peak, it is slightly higher than the previous linear case due to the decreased inductance. After a few seconds, the temperature reaches 40 °C; the corresponding current remains triangular, as in Fig. 8. Figure 9 represents the situation after 20s where the inductor temperature is 60 °C, Fig. 10 after 40s (temperature 80 °C), Fig. 11 after 66s (temperature 100 °C), Fig. 12 after 92s (temperature 120 °C), Fig. 13 after 120s (temperature 140 °C), and finally, Fig. 14 after 134s (temperature 150 °C). This last temperature strongly exceeds the maximum allowable one forcing to stop the test.

The figures from 7 to 14 give the different profiles of the current starting from a triangular shape and gradually becoming cusp-like. It can be noted that the mean value of the current does not vary; differently, its peak raises of about 15%. This shows that the increase in temperature forces the inductor into a non-linear operating condition. Besides, the higher peak-to-peak value of the current implies an increase of the RMS value of the current that augments the Joule losses.

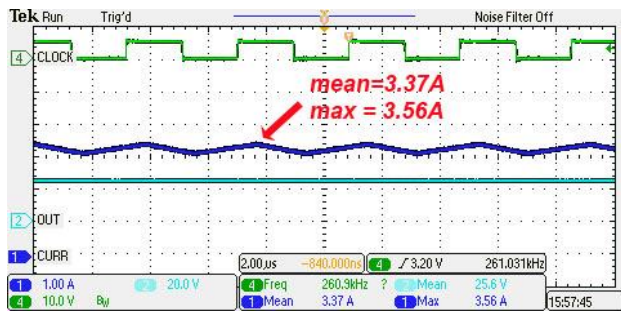


Fig. 7. Output voltage and inductor current at the beginning of the test in non-linear operation with a temperature of 29.4 °C (environment).

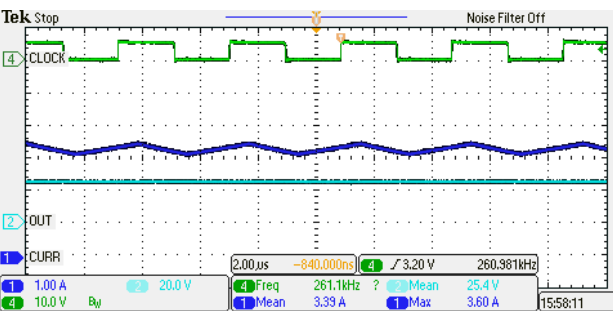


Fig. 8. Output voltage and inductor current during the test in non-linear operation when the temperature is 41 °C.

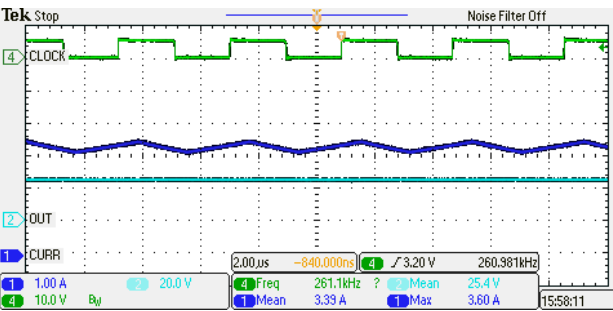


Fig. 9. Output voltage and inductor current during the test in non-linear operation when the temperature is 60 °C.

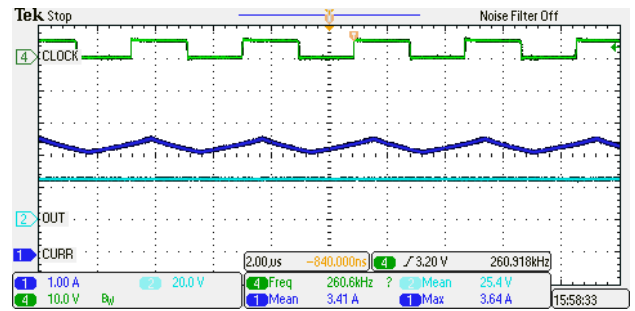


Fig. 10. Output voltage and inductor current during the test in non-linear operation when the temperature is 80 °C.

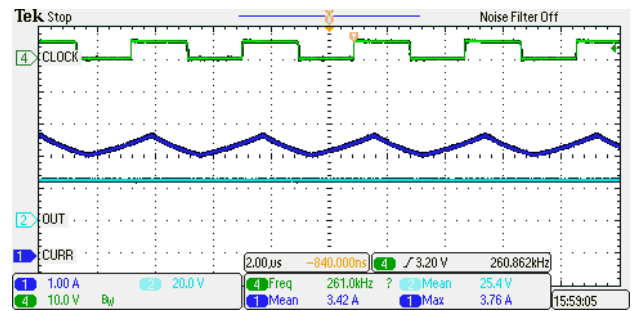


Fig. 11. Output voltage and inductor current during the test in non-linear operation when the temperature is 100 °C.

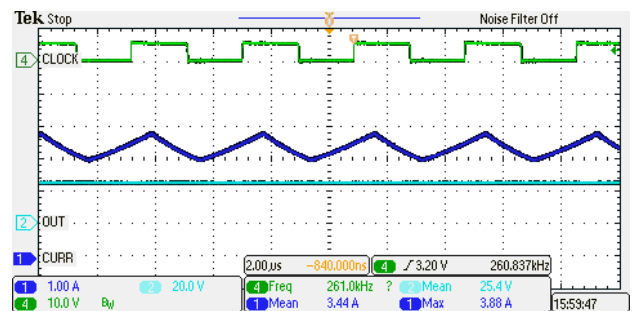


Fig. 12. Output voltage and inductor current during the test in non-linear operation when the temperature is 120 °C.

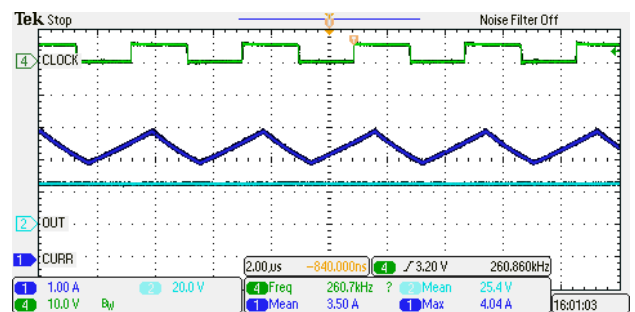


Fig. 13. Output voltage and inductor current during the test in non-linear operation when the temperature is 140 °C.

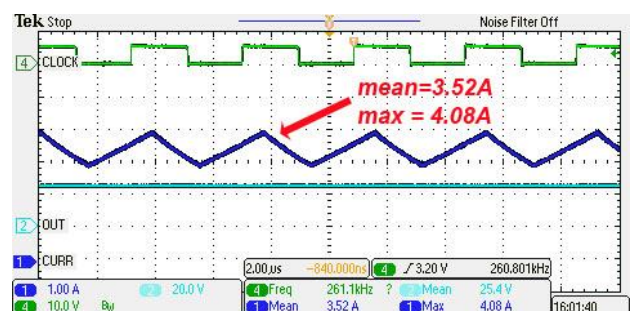


Fig. 14. Output voltage and inductor current during the test in non-linear operation when the temperature is 150 °C.

From the graph of Fig. 15, reproducing the core temperature versus time, the unstable trend can be detected when eq. (8) is not satisfied.

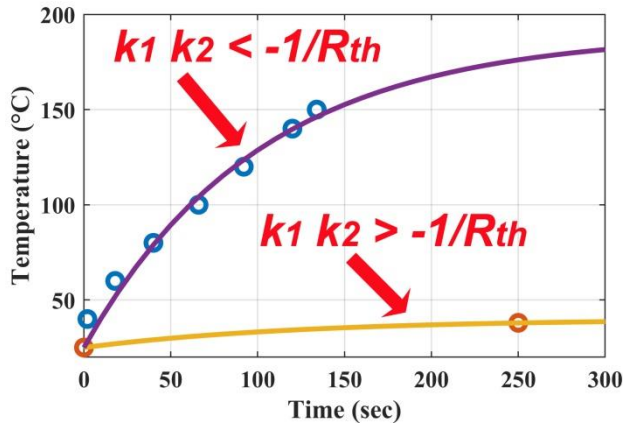


Fig. 15. The evolution of the core temperature over time based on eq. (8).

The influence of the core temperature on the inductor current waveform can be appreciated by comparing its AC component acquired at environmental temperature and at 150 °C, shown in Figs 16 and 17 respectively. It is evident that the final waveform shape differs from the traditional triangular waveform. An increase of the current peak of about 150% occurs. Besides, for temperature up to 60 °C no significant variation of the current shape is noticed; on the contrary, as early as 80 °C the contribution of nonlinearity can be seen, which causes a deformation of the current and an increase in the maximum value. From this point the temperature diverges.

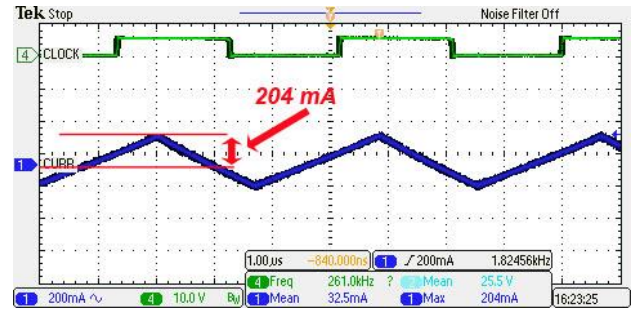


Fig. 16. AC component of the inductor current at environmental temperature.

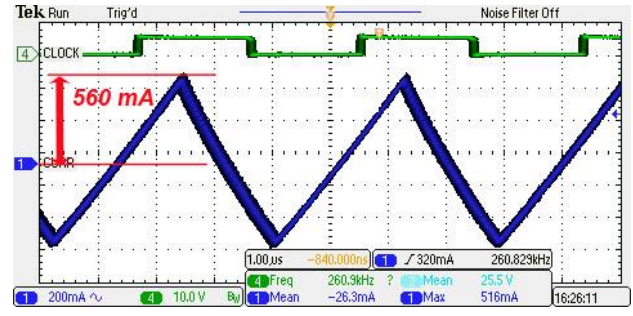


Fig. 17. AC component of the inductor current at 150 °C when the test has been stopped; it is evident the distortion and the increase in the peak.

5. Thermal Analysis

During operation the inductor experiences a power dissipation with consequent increase of the temperature. As explained in the previous section, it can become unstable exceeding the maximum temperature allowed by manufacturer. The thermal analysis exhibited in Fig. 18 shows that the maximum inductor temperature is found on the copper winding; this shows that the Joule losses are greater than the magnetic losses and result in the heating of the inductor as assumed in eq. (4). The inductor's temperature exceeds the power switch temperature, hence it is heated by the inductor.

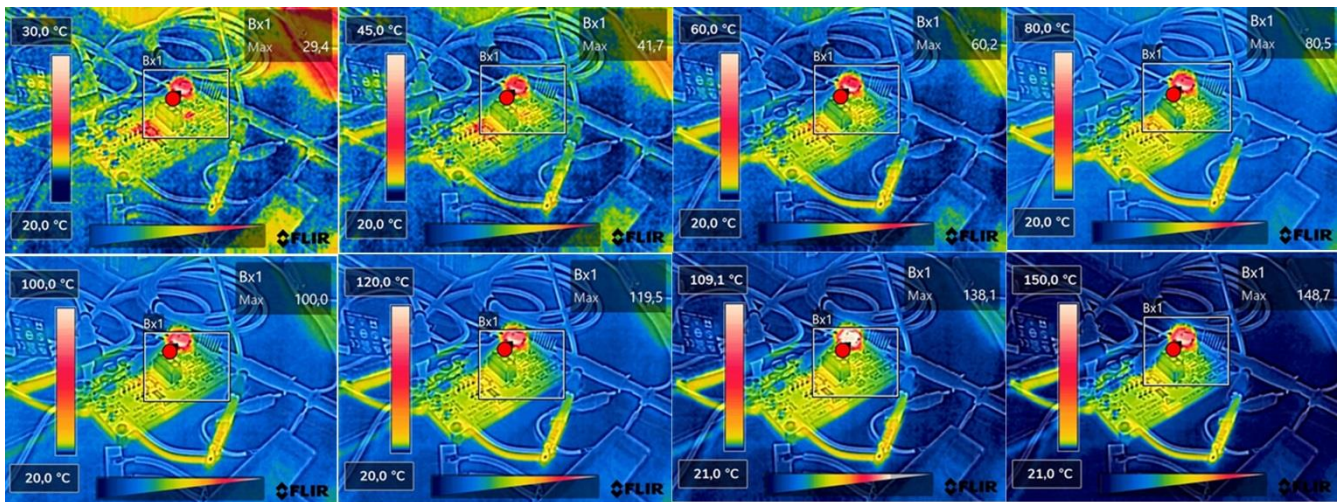


Fig. 18. Thermal evolution of the inductor's temperature during operation.

The heating, although tolerated by the inductor, increases the temperatures of other circuit components and of the PCB.

6. Conclusion

The operation in the non-linear zone of a power inductor can excite an unstable behavior that depends on the load current and the thermal resistance of the inductor. A stability limit condition has been retrieved in this paper. The parameters belonging to the stability condition were determined analytically as a function of the converter load current. A suitable case study demonstrated that the failure to meet the stability condition leads the core temperature outside its safe operating area and increases the temperature of the other components, including the PCB. This study showed that the design of SMPS with a power inductor in non-linear operation must consider both the thermal model and load current to avoid thermal runaway.

Acknowledgment

This research was partially funded by the ECSEL-JU project REACTION (first and euRopEAn siC eigTh Inches pilOt liNe), Grant Agreement No. 783158.

References

- [1] Perdigão, M.S.; Trovão, J.P.F.; Alonso, J.M.; Saraiva, E.S. Large-Signal Characterization of Power Inductors in EV Bidirectional DC-DC Converters Focused on Core Size Optimization. *IEEE Trans. Ind. Electron.* 2015, 62, 3042–3051. <https://doi.org/10.1109/TIE.2015.2402632>.
- [2] Kaiser, J.; Durbaum, T. An Overview of Saturable Inductors: Applications to Power Supplies. *IEEE Trans. Power Electron.* 2021, 36, 10766–10775. <https://doi.org/10.1109/TPEL.2021.3063411>.
- [3] Oliveri, A.; Lodi, M.; Storace, M. Nonlinear Models of Power Inductors: A Survey. *Int. J. Circuit Theory Appl.* 2022, 50, 2–34. <https://doi.org/10.1002/cta.3147>.
- [4] Di Capua, G.; Femia, N. A Novel Method to Predict the Real Operation of Ferrite Inductors with Moderate Saturation in Switching Power Supply Applications. *IEEE Trans. Power Electron.* 2016, 31, 2456–2464. <https://doi.org/10.1109/TPEL.2015.2438952>.
- [5] Scirè, D.; Vitale, G.; Ventimiglia, M.; Lullo, G. Non-Linear Inductors Characterization in Real Operating Conditions for Power Density Optimization in SMPS. *Energies* 2021, 14, 3924. <https://doi.org/10.3390/en14133924>.
- [6] Scirè, D., Lullo, G., & Vitale, G. (2022). Non-Linear Inductor Models Comparison for Switched-Mode Power Supplies Applications. *Electronics*, 11(15), 2472.
- [7] Lullo, G.; Scirè, D.; Vitale, G. Non-Linear Inductor Modelling for a DC/DC Buck Converter. *Renew. Energy Power Qual. J.* 2017, 1, 686–693. <https://doi.org/10.24084/repqj15.433>.
- [8] Scirè, D.; Vitale, G.; Ventimiglia, M.; Lullo, G. Non-Linear Inductors Characterization in Real Operating Conditions for Power Density Optimization in SMPS. *Energies* 2021, 14, 3924. <https://doi.org/10.3390/en14133924>.
- [9] Detka, K.; Gorecki, K.; Zarebski, J. Modeling Single Inductor DC-DC Converters with Thermal Phenomena in the Inductor Taken into Account. *IEEE Trans. Power Electron.* 2017, 32, 7025–7033. <https://doi.org/10.1109/TPEL.2016.2628202>.
- [10] Vitale, G.; Lullo, G.; Scire, D. Thermal Stability of a DC/DC Converter With Inductor in Partial Saturation. *IEEE Trans. Ind. Electron.* 2021, 68, 7985–7995. <https://doi.org/10.1109/TIE.2020.3014580>.
- [11] Scirè, D.; Lullo, G.; Vitale, G. EMI Worsening in a SMPS with Non-Linear Inductor. *Renew. Energy Power Qual. J.* 2022
- [12] Scire, D.; Lullo, G.; Vitale, G. EMI Filter Re-Design in a SMPS with Inductor in Saturation. In Proceedings of the 2021 IEEE 15th International Conference on Compatibility, Power Electronics and Power Engineering (CPE-POWERENG), Florence, Italy, 14–16 July 2021; pp. 1–7.
- [13] Texas Instruments LM5122EVM-1PH Wide Vin Synchronous Boost Controller Evaluation Module Available online: <https://www.ti.com/tool/LM5122EVM-1PH> (accessed on 14 June 2022).
- [14] Coilcraft Inc., “SMT Power Inductors - DO5010H Series,” 2020. <https://www.coilcraft.com/en-us/products/power/unshielded-inductors/ferrite-drum-surface-mount/do/do5010h/> (accessed Sep. 01, 2020).